Rapid rebalancing of co-tuned ensemble activity in the auditory cortex

HiJee Kang[1], Travis A. Babola[1], & Patrick O. Kanold[1,2*]

Affiliations:

[1] Department of Biomedical Engineering, Johns Hopkins University, Baltimore, MD 20215

[2] Kavli Neuroscience Discovery Institute, Johns Hopkins University, Baltimore, MD 20215

*Corresponding author. Email: pkanold@jhu.edu

Keywords: cortex, optogenetics, holography, balance, plasticity

Abstract: Sensory information is represented by small neuronal ensembles in sensory cortices. Neuronal activity shows high trial-by-trial variability in that repeated presentation of the same stimulus, e. g., multiple presentations of the same sound activate differing ensembles in the auditory cortex (AC). How the differing ensembles interact to selectively activate to process incoming sound inputs with reduced energy is unknown. Efficient processing of complex acoustic signals requires that these sparsely distributed neuronal ensembles actively interact in order to provide a constant percept. Here, we probe interactions within and across ensembles by combining *in vivo* 2-photon Ca^{2+} imaging and holographic optogenetic stimulation to study how increased activity of single cells level affects the cortical network. We stimulated a small number of neurons sharing the same frequency preference alongside the presentation of a target pure tone, further increasing their tone-evoked activity. We found that other non-stimulated co-tuned neurons decreased their tone-evoked activity while non co-tuned neurons were unaffected. This shows that co-tuned ensembles communicated and balanced their total activity across the network. The rebalanced activity due to external stimulation remained constant. These effects suggest that co-tuned ensembles in AC interact and rapidly rebalance their activity to maintain encoding homeostasis, and that the rebalanced network is persistent.

Main Text

Sensory perception requires fast encoding of relevant stimuli from a mixture of complex signals. Sensory cortices play a vital role for such sensory processing. In the auditory domain, for example, small neuronal ensembles the auditory cortex (AC) are actively engaged to efficiently perceive relevant acoustic information [1-4]. The AC contains multiple ensembles of neurons [5-7] and difference ensembles of neurons activate together in response to repeated presentation of the same acoustic input, e.g., tones of the same frequency [5,8-10], referred to co-tuned neurons. Activation of these different subsets of co-tuned neurons at each presentation of a stimulus reflects sparse encoding of stimuli. Such sparse representation of co-activated neurons enables efficient coding with reduced energy to process complex information [11-16].

This sparse neuronal representation raises key questions about how the overall activity within the cortical network is balanced across ensembles of co-tuned neurons. In particular, when a specific sound is present, a subset of co-tuned neurons will be activated, but not all co-tuned neurons [17]. Given that the percept of a repeating stimulus is constant, we speculated that their activity is balanced across co-tuned as well as non co-tuned ensembles.

While neuronal ensembles constantly update their activities based on incoming information, how the activation of a particular sparse neuronal ensemble affects other neurons within the network to maintain the overall network balance for processing specific sensory information *in vivo* is largely unknown. *In vivo* holographic optogenetic stimulation studies in the visual cortex (VC) suggested that inhibitory processes play a role in balancing overall network activity. *In vivo* single-cell holographic stimulation resulted in changes in neighboring non-targeted neurons' response amplitudes in the primary visual cortex (V1) [18], with similarly tuned neurons' activity being suppressed. Moreover, *in vivo* holographic optogenetic stimulation observed that visually-suppressed neurons' attenuated response amplitudes when holographic stimulation was given along with the visual stimulus presentation, which was not the case for visually activated neurons [19]. This suggested supralinear-to-linear input-output (IO) functions of neurons *in vivo*, rather than threshold-linear IO functions observed *in vitro*. From these studies, inhibitory influence from extra neuronal activation in the VC seems to play a major role during *in vivo* sensory processing, likely to maintain the overall activity balance of the network.

The local frequency preference in the auditory cortex is diverse, thus neighboring neurons can show widely differing tuning properties [5]. To test how activity in specific cells among an intermingled and spatially distributed co-tuned and non co-tuned cell population is balanced during auditory processing, we stimulated a small group of cells using *in vivo* holographic optogenetic stimulation method [20,21] while imaging AC population activity using 2-photon Ca^{2+} imaging in awake mice. Stimulating small ensembles of co-tuned neurons together with the presentation of a pure tone in their preferred frequency increased their tone-evoked activity. Moreover, we observed that non-stimulated co-tuned neurons decreased their tone-evoked activity. Non co-tuned ensembles did not show such changes in tone-evoked responses. Thus, the increased activity in the stimulation-targeted ensemble had caused the decreased activity in the non-stimulated co-tuned ensembles, specifically when the stimulation-paired pure tone was their preferred frequency. Non-targeted co-tuned neurons showing such effects were not necessarily neighboring cells to targeted cells, suggesting These results suggest that co-tuned ensembles form interacting networks that balance their activity.

Optogenetic holographic stimulation increases activity in small ensembles *in vivo*

In order to sparsely manipulate neuronal ensembles, we aimed to stimulate a small ensemble of five co-tuned cells. To achieve reliable and selective *in vivo* holographic optogenetic stimulation of small ensembles of neurons with single cell precision, we generated an AAV co-expressing the red-shifted opsin rsChRmine and GCaMP8s (AAV9-hSyn-GCaMP8s-T2A-rsChRmine). Injecting AAV9-hSyn-GCaMP8s-T2A-rsChRmine into AC

yielded cells expressing both GCaMP and opsin (Fig. 1A). We first tested holographic stimulation, on a single target cell or five cells simultaneously over the AC, to validate stimulation efficiency and reliability. For single cell stimulation, varying the stimulation point from a target cell position by 10, 20, and 30 µm along either x-axis or y-axis of the fields of view (FOV; n = 15 cells, 3 animals) showed a rapid decay of response amplitudes to stimulation by the distance shift from the original cell position, confirming reliable holographic stimulation at the single-cell level (~15 µm diameter) (mixed-effect model, $p < 0.05$; Fig. 1B). For 5-cell stimulation, cells could reliably be photo-stimulated *in vivo* (5 mW/cell, 15 µm spiral, 30 revolutions, 6 s inter-stimulus interval (ISI), 5 trials) and exhibited robust Ca^{2+} responses (Fig. 1CD; permutation test, all $p < 0.05$), comparable with responses to other opsins [22-25]. Thus, *in vivo* holographic stimulation allows us to target and precisely increase the activity of groups of single neurons in AC.

Optogenetic holographic stimulation increases sound evoked activity in A1 ensembles

We next sought to investigate how increased neural activity in small co-tuned ensembles during sound presentation affected sound-evoked responses in targeted and non-targeted co-tuned and non co-tuned ensembles. To do so, we first needed to identify the tuning properties of single neurons and then target a subset of co-tuned neurons for stimulation. To study how increased activity of a small number of neurons influences the activity of other neurons based on their frequency tuning properties, we designed an experimental paradigm comprising four sequential imaging sessions (Fig. 2):

First, in the cell selection session (Fig 2), we identified tuned ensembles in primary auditory cortex (A1) layer 2/3 (L2/3) by assessing frequency tuning properties of neurons within the FOVs covering 550 μm^2 (total cells = 7344, sound responsive cells = 1331, FOVs = 23; Fig. 1D). We presented pure tones of three different frequencies spanning the hearing range of the mouse (4 kHz, 16 kHz, and 54 kHz, 100 ms duration, 2 sec. ISIs, 10 repeats for each frequency). We chose 16 kHz and 54 kHz as the representative target ensemble frequency, as 16 kHz is within the most sensitive frequency range of mice [26] and 54 kHz is within the range of mouse ultrasonic vocalization [27]. For the 16 kHz target ensemble condition, we then selected five cells (*target cells*) among the top 30% most responsive cells to a 16 kHz tone. Similarly, for the 54 kHz target ensemble condition, we selected five target cells among the top 30% most responsive cells to a 54 kHz tone. By selecting target cells sharing the same frequency preference, we aimed at investigating distinct activity changes from co-tuned neuronal ensembles for processing the target frequency. By selecting target ensembles in two different frequencies, we ensured that effects of stimulation were not specific to one particular population.

Second, in the baseline session (Fig 2), we determined the sound-evoked responses of imaged cells by presenting a series of 16 kHz and 54 kHz pure tones in a random order (100 ms duration, 5.8-6.5 sec. ISI; baseline session, 30 repeats for each frequency). Exemplar responses of cells from a 16kHz and 54kHz ensemble are shown as black traces in Figure 3B and 3E.

Third, in the stimulation session (Fig 2), we examined how cells change their responses when a small group of cells in the network increases their activity, we presented the same tones, in tandem with the optogenetic stimulation of five target cells (stimulation session, 100 ms stimulation duration). We performed different sessions for the 16 kHz and 54 kHz target ensembles (18 FOVs for 16 kHz target ensemble condition and 12 FOVs for 54 kHz target ensemble condition). Figure 3A and D show 2 example FOV with targeted neurons for a 16kHz and 54 kHz ensemble.

Since both imaging and optogenetic stimulation involves optomechanical components we wanted to ensure that effects were not due to artifacts causes by our stimulation or imaging setup. Moreover, cells can adapt their responses to repeated sound presentation. Thus, we added

an additional control condition. For this control condition, we performed the "stimulation" session with 5 target cells but with 0 mW laser power (i.e., no stimulation) to verify that any response changes occurring in the stimulation session compared to the baseline session were not simply due to the eventual response adaptation of neurons to the tuned frequency (control condition; 13 FOVs). By selecting cells and presenting 0 mW laser power, instead of no target cell selection or selecting any other no-cell area within the FOV, we ensured that the laser power given to selected cells was the only difference between the actual stimulation and control conditions, keeping any noise caused by the imaging and stimulation setup the same.

Fourth, after the stimulation session (Fig 2), we performed an additional imaging session (post-stimulation session), presenting another series of 16 kHz and 54 kHz pure tones in a random order to examine whether changes in the sound-evoked responses persisted or reverted back after the stimulation session.

We first identified the effect of the optogenetic stimulation on the targeted ensembles. Figures 3A and 3D show fluorescence traces of exemplar cells from 16kHz and 54kHz target ensembles. Optogenetic stimulation increased the sound evoked fluorescence amplitude in these individual cells. To quantify the effect of the optogenetic stimulation, we compared the tone-evoked fluorescence responses of the targeted cells with and without stimulation (Stimulation effect = $\Delta F/F_{(stimulation\ session)} - \Delta F/F_{(baseline\ session)}$). Around 72% of target cells (66 out of 90 cells over 18 FOVs for 16 kHz target stimulation and 42 out of 60 cells 12 FOVs for over 54 kHz target stimulation) showed increased response amplitude during the stimulation session compared to the baseline session, regardless of the tone presented (Fig. 3BD; permutation tests, all $p < 0.001$). These results indicate that holographic stimulation was able to reliably increase activity in small populations of neurons. Moreover, given that the target cells we selected were more responsive to a specific frequency, this increase in fluorescence indicates that the cells' responses to their preferred tone were not saturated.

Optogenetic holographic stimulation decreases activity in non-targeted co-tuned ensembles

We next investigated if the optogenetically increased sound-evoked activity of a small group of stimulated cells might lead to activity changes in other non-targeted cells. During holographic optogenetic stimulation of the targeted cells, the non-targeted, but sound-responsive cells (n = 945 cells for 16 kHz target ensemble condition and n = 465 cells for 54 kHz target ensemble condition), also changed their activity, showing either increased or decreased response amplitudes (Fig. 3AD).

If cortical networks rebalance their activity, we speculated that in increased tone evoked activity in the targeted ensemble would lead to a decrease in tone evoked activity in coupled ensembles such that the overall activity. Moreover, if such rebalancing occurs, such re-balancing would be performed for distinct acoustic inputs related to the cell's tuning property. For example, stimulation of a 16kHz ensemble would lead to a larger decrease in the response of the 16kHz tone response than the 54 kHz tone response of other non-stimulated 16kHz cells.

To address these questions, we investigated if the increased activity in the targeted cells affected activity in non-targeted cells and how these changes related to the tuning properties of the cell. We first defined each sound-responsive cell's frequency selectivity by computing a difference between response amplitude to 16 kHz and 54 kHz from the baseline session (frequency preference = $(\Delta F/F_{(16kHz)}) - (\Delta F/F_{(54kHz)})$). We sub-grouped these cells into either 16 kHz preferring or 54 kHz preferring cell groups, taking 0 (i.e., no preference) as a criterion (Fig. S1). Two subgroups showed greater tone evoked responses to their preferred frequency, regardless of conditions ($t(5700) = 4.79$, $p < 0.0001$; Fig. 4). This confirms that the criterion for cell group threshold is valid.

We then focused on our main question by comparing the stimulation effect of two target ensembles groups to the control condition to further identify whether the stimulation induced

further response decrease on non-target co-tuned neurons. Since neural activity in AC rapidly shows stimulus-specific adaptation to the repeated presentation of the stimulus, we used response amplitude change between baseline and "stimulation" control session as a representative threshold to test the effect of the stimulation. We again used the response amplitude difference between the baseline and stimulation sessions as the stimulation effect ($\Delta F/F_{(stimulation\ session)} - \Delta F/F_{(baseline\ session)}$). We removed outlier cells by taking 3 standard deviations from median response amplitudes across cells as a criterion. By doing so, we eliminate nearby cells (e.g., cells that are within 20-30 μm distance from the target stimulation point) that may have changed their activities due to a more direct effect of stimulation. We first examined the stimulation effect between non-targeted co-tuned and non co-tuned cells for each condition (both 16 kHz and 54 kHz target ensembles and control conditions). For both 16 kHz (n = 521 cells) and 54 kHz preferring non-targeted cell groups (n = 403 cells), we observed greater response amplitude decrease when their preferred frequency pure tone was presented, e.g., 16 kHz tones for 16 kHz cells ($F(1,2196) = 165.04$, $p < 0.0001$) or 54 kHz tones for 54 kHz cells ($F(1,1827) = 211.35$, $p < 0.0001$), due to the stimulus-specific adaptation similar to the control condition (Fig 5A left columns, solid symbols).

More importantly, when compared non-targeted 16 kHz preferring cells (n = 521 cells) across conditions, we observed a further response amplitude decrease for 16 kHz tone presentation from 16 kHz target ensemble condition compared to the control condition ($t(39) = -2.62$, $p = 0.01$), while 54 kHz preferring cells did not show decreased response amplitudes for 16 kHz tone presentation compared to the control condition ($t(39) = 0.09$, $p = 0.92$; Fig. 5A middle columns). These results show that the increased activity in target stimulated cells resulted the decreased activity in non-stimulated co-tuned (16 kHz preferring) cells. The effect of holographic optogenetic stimulation of 16 kHz cells has the strongest effect on 16 kHz responses in non-stimulated 16 kHz preferring cells.

Manipulating neural activity of 54 kHz target ensemble condition yielded similar results (Fig. 5A right columns). Response amplitude decrease for 54 kHz tone presentation from 54 kHz preferring cells (n = 244 cells) were further decreased compared to the control condition ($t(39) = -2.52$, $p = 0.016$). No response amplitude change for 16 kHz tone presentation was observed, compared to the control condition ($t(39) = 0.36$, $p = 0.72$). These results indicates that the effect of holographic optogenetic stimulation does not depend on the certain tuning of cells, but on the co-tuning between stimulated and non-stimulated neurons. Also, such effect is not driven by only a small number of non-target cells with great response changes. Rather, the overall population of cells show relative response changes due to the stimulation when synchronized with their preferred frequency.

Overall, these results further suggest that when neural activity is increased in a subset of target cells by photostimulation in addition to the target sound presentation, other co-tuned cells selectively reduce their tone-evoked responses to their preferred tone presentation, suggesting that the network rebalances to maintain network activity within a certain range.

Rebalanced network responses are stable

We then questioned whether such response amplitude changes due to stimulation within the local network is persistent. To test whether the rebalanced status of the neuronal ensemble is persistent, we next examined the tone-evoked response amplitude changes from the post-stimulation session compared to the stimulation session (post-stimulation effect: $\Delta F/F_{(post-stimulation\ session)} - \Delta F/F_{(stimulation\ session)}$). Response amplitudes were similar between conditions and tone presentation frequency for both groups of cells ($F(2, 4056) = 1.83$, $p = 0.16$; Fig. 5B). These results indicate that pairing exogenous stimulation of a subset of neurons with sounds can instantaneously change the network responses to sounds, and this change can persist at least for many minutes during the experimental session.

Sparsely distributed non-targeted co-tuned ensembles immediately rebalance their activities to maintain homeostatic balance of the network

Network homeostasis can be achieved by multiple mechanisms operating on a different timescale. Thus, to get insights into potential mechanisms underlying the observed rebalancing, we next investigated how rapidly cells start adjusting their responses during the stimulation condition. We examined the stimulation effect (response amplitude changes due to stimulation of targeted cells) for non-targeted co-tuned ensembles at a single trial level. We observed decreased response amplitudes from the first trial, without any significant decay across trials (Fig. 6A), regardless of cell groups, frequency presentation, and conditions (sum-of-squares F-test, all $p > 0.05$). Specifically, the lack of trial-related response amplitude changes for non-targeted co-tuned ensembles indicates that non-targeted co-tuned cells immediately change their activity whenever targeted cells increased their activity due to stimulation, to maintain homeostatic balance of the network.

Activity rebalancing could be driven by local, e.g. changes in excitatory-inhibitory (E/I) balance [28], or distributed changes. To identify whether co-tuned ensembles that changed their activities are locally or widely distributed, we computed the minimum distance of each non-targeted cell to any of the targeted cells. For the stimulation condition, we excluded neighboring non-targeted cells that were within 15 μm distance of the targeted cells as their increased response amplitudes (sum-of-squares F-test, $p < 0.05$) could have been at least partially due to photostimulation effects (Fig. 1B-D). We observed that non-target co-tuned ensembles were widely distributed within the FOV, similar to non-target non co-tuned ensembles as well as those from the control condition (sum-of-squares F-test, $p > 0.05$; Fig. 6B). This indicates that activity changes of non-targeted co-tuned ensembles are not simply due to direct input changes of cells from external stimulation within a tight localized network. Rather, sparsely represented widespread co-tuned ensembles constantly update incoming information based on their functional tuning properties.

Response changes are not limited to neurons with specific characteristics

Based on the findings of rebalanced cortical network, we next aimed to identify characteristics of those non-stimulated co-tuned neurons such as tuning sensitivity or their firing rate. First, we tested whether cells with highly tuned to one frequency than another show greater response amplitude changes. We computed a linear regression on response amplitude change relative to frequency preference index $(\Delta F/F_{(16kHz)}) - (\Delta F/F_{(54kHz)})$ across cells for each frequency preferring cell groups and each target ensemble condition. While cells with greater frequency preference show greater response decrease regardless of conditions, we observed no clear interaction between the frequency preference and stimulation effect nor the interaction between baseline response amplitude and stimulation effect (Fig. 7A; ANCOVA, all $p > 0.05$) across preferring cell groups and target ensemble conditions. We then tested whether the stimulation effect is related to the baseline response amplitude (i.e., spiking rate of the cells). Again, we observed no significant difference between cell groups and tone frequency, suggesting that stimulation effect that is specific to the preferring frequency is not necessarily driven by specific group of cells (Fig. 7B; ANCOVA, all $p > 0.05$). These results indicate that response amplitude changes occur to most of relevant neurons, instead of only to a specific subset of those non-targeted co-tuned neurons.

Discussion

Trial-by-trial variability in neuronal activity is ubiquitous in the brain and how sensory-evoked activity is distributed across co-tuned networks has been unknown. Here, we leveraged the capability for selective, *in vivo* stimulation by holographic optogenetics to investigate how functionally related neuronal ensembles in AC coordinate their activities. Our results show that manipulating the activity of a small subset of co-tuned neurons can change the auditory-evoked

responses of other co-tuned neurons. Thus, increased activity in one subset of neurons is balanced by a decrease in activity in the remainder of the co-tuned population of neurons. Importantly, such network rebalancing occurs only for processing a specific acoustic feature relevant to their tuning. These findings suggest that neuronal ensembles with strengthened connectivity established from past experiences actively interact and update their status to maintain the overall network, enabling energy efficient sensory processing.

The present work applied holographic optogenetic stimulation to manipulate neuronal activities at a single-cell resolution for the first time in AC. Similar to neuronal activity changes in VC from previous studies [18,19], our study further supports inhibitory influence on a subset of neurons due to the extra activation within the network. In the VC, single cell stimulation resulted in suppression of neighboring co-tuned neurons [18]. Our results here show that feature specific suppression exists in widely spatially scattered ensembles of non-targeted co-tuned neurons. The widely distributed response amplitude decreases we observe suggest that such phenomenon does not only originate from local neighboring cells of the targeted area but must involve widespread networks. Thus, the effect we observe is not simply due to inhibition caused by neighboring interneurons from the optogenetic stimulation. Instead, neurons sharing similar functional characteristics that are sparsely represented within AC actively interact overall.

On short timescales, recurrent cortical networks are thought to update their activities based on incoming information to homeostatically rebalance overall activity [29,30]. In contrast, on long timescales, co-activated neurons processing the same functional acoustic properties strengthen their connectivity by Hebbian learning [31-33]. Thus, rather than by a single dominant mechanism, cortical networks are formed by an active interaction between homeostasis and Hebbian learning [34-37]. Rebalancing of network activity is often explained by homeostatic rebalancing of individual cell's activity [30,38] or an E/I balance: increased activity of inhibitory neurons resulting in reduced activity of excitatory neurons [28]. Our results suggest that rebalancing is tuning-specific. Given that inhibitory neurons in A1 tend to be generally less frequency selective than excitatory neurons [39], it is unlikely that changes in inhibition are a major contributor to the observed effect. While our AAV was not cell-type specific, it is also unlikely that many selected target neurons would be inhibitory interneurons as a greater proportion of neurons in sensory cortices are excitatory (about 80% compared to 20% inhibitory [40-43]; AAV-hSyn expresses in a similar proportion of excitatory and inhibitory neurons [44]). Furthermore, our primary cell selection criterion for stimulation yielded a subgroup of strongly tone-responsive cells (top 30% of cells that show the biggest evoked responses to the target tone). With this criterion, it is likely that we included mainly excitatory neurons since excitatory neurons generally show greater sound-evoked responses than inhibitory neurons [45,46]. Moreover, re-occurring sounds evoke activity changes of excitatory and inhibitory neurons in the same direction, thus resulting in no change in E/I balance [45,47], suggesting that balancing mechanisms beyond changes in E/I balance exist such as short-term depression at thalamocortical synapses [48].

In contrast to slow changes of homeostatic plasticity for the E/I balance, homeostatic changes in cortical cellular responses can occur fast and are cell-specific, thereby tuned to their functional response properties [49-51]. Thus, we speculate that our results of non-target neurons decreasing their response amplitudes are likely due to the homeostatic response changes of excitatory cells rather than changes in E/I balance.

Lastly, no further response change was observed in the post-stimulation session indicating that the rebalanced network status remained constant. Indeed, constant amplitudes in the post-stimulation session were observed regardless of conditions, subgroups, and frequencies, suggesting that the network status persistence was achieved due to repeatedly presented acoustic stimuli and stimulation. The persistence after the stimulation condition further suggests that once the newly learned rebalanced network status is achieved, the network

response is stabilized which remains persistent. The mechanisms behind this stabilization are unclear but might indicate an interactive interplay of homeostasis and Hebbian learning to form co-active networks [52].

Taken together, the present study reveals how the neuronal ensembles in AC constantly rebalance to maintain a homeostatic processing equilibrium for a given sensory input, and that rebalanced networks remain persistent. The network activity can be controlled by even a small subset of neurons, and the network change is highly related to the functional tuning properties of neurons.

Materials and Methods

Methods

Animals

A total of 14 mice over 8 weeks old (8 – 30 weeks, 6 males and 8 females) were used for the experiments. To retain high-frequency hearing at experimental ages, offspring from C57BL6/J and B6.CAST-*Cdh23*$^{Ahl+}$/Kjn (Jax 002756) were used for all experiments. Animals were housed on 12 hr reversed light/dark cycle. All experimental procedures were approved by Johns Hopkins Institutional Animal Care and Use Committee.

Preparation of AAV9-hSyn-GC8s-T2A-rsChRmine

To generate AAV9-hSyn-GC8s-T2A-rsChRmine virus, a gene fragment containing T2A, rsChRmine, Kv2.1 soma-targeted localization motif, and 3xHA tag (synthesized by Twist Biosciences) was subcloned into the pGP-AAV-syn-jGCaMP8s plasmid vector (Addgene: 162374). Viral vectors were commercially prepared (Virovek) to a concentration of 1e+13vg/mL.

Surgery and virus injection

Surgery was performed as previously described [9,10]. We injected dexamethasone (1mg/kg, VetOne) subcutaneously (s.c.) to minimize brain swelling prior to surgery. 4% isoflurane (Fluriso, VetOne) with a calibrated vaporizer (Matrix VIP 3000) was used to induce anesthesia, and then was reduced down to 1.5 – 2% to maintain the anesthesia. Body temperature was monitored to be maintained at around 36°C throughout the surgery (Harvard Apparatus Homeothermic monitor). We first removed hair on the head using a hair removal product (Nair) to expose the skin. Betadine and 70% ethanol were applied 3 times on the exposed skin. Skin and tissues were then removed, and muscles were scraped to expose the left temporal side where the craniotomy was conducted. Unilateral craniotomy was performed to expose about 3.5 mm diameter region over the left AC. Virus (AAV9-hSyn-GC8s-TSA-rsChRmine titer of 1:2) injection was performed at 2-3 sites near tentative A1 area at about 300 µm depth from the surface, using a glass pipette controlled by a micromanipulator (Sutter Instrument MPC-200 and ROE-200 controller). We injected 300 nL on each site at the rate of 180 nL/min (Nanoject3). Once virus injection was completed, two circular glass coverslips (one of 3 mm diameter and one of 4 mm) were affixed with a clear silicone elastomer (Kwik-Sil, World Precision Instruments). An extra layer of dental acrylic (C&B Metabond) was applied around the edge of the cranial window was applied to further secure the window, cover the exposed skull, and adhere a custom 3D-printed stainless steel headpost. Carprofen (5 mg/kg) and cefazolin (300mg/kg) were injected (s.c.) post-operatively. Animals had 3-4 weeks of recovery and viral expression time before any imaging was performed.

Experimental procedures

Animals were head-fixed on a custom-made stage, where a free field speaker (TDT ED1) was faced towards the right ear at 45 degrees. All sound stimuli were driven by TDT RX6 multiprocessor and we imaged GCaMP8s responses with a resonant scanning two-photon

microscope (Bruker Ultima 2Pplus; 940 nm excitation wavelength) at A1 L2/3 (160 – 200 μm). A1 was identified by its tonotopy gradient using widefield imaging [53]. During 2-photon imaging sessions, we first conducted a short imaging session (about 1 min.) presenting 100-ms pure tones at 3 different frequencies (4, 16, 54 kHz) at 70 dB SPL, covering the mouse hearing range, for 10 times each in a randomized order (ISI: 2 sec). This was to identify initial tuning properties of sound-responsive cells (cell selection session). The acquired imaging data was immediately processed using 'suite2p' and a custom-written Matlab script to identify tone-responsive cells for each frequency. We continued only when at least 50% of cells within the FOV showed sound-evoked responses. We took 16 kHz or 54 kHz as our target functional properties. Target frequency was randomly assigned. We manually tested the response changes to stimulation of the top 30% of target frequency responsive cells (~ 20 cells) selected from the cell selection session by using a stimulation laser (Light Conversion Carbide; 1040 nm excitation wavelength). Stimulation laser power was set around 5 mW per cell. We selected 5 representative cells (target cells) that showed visible fluorescence changes to the stimulation.

Prior to the main experimental session, we ran a short (~ 1 min.) stimulation session without any sound presentation that comprised 5 trials of 100-ms stimulation with 6-second ISIs for a rapid check of the stimulation effect. This session was restricted to 5 trials of stimulation given the limited time of the imaging session, leading to larger variability of the observed stimulation effect. We further verified the stimulation effect from the experimental stimulation session where 30 trials were given.

For the main experiment, three consecutive imaging sessions were followed by the presentation of either 16 kHz or 54 kHz 100 ms pure tones with random ISIs between 5.8 – 6.5 sec. for 30 trials each, as baseline session, stimulation session, and post-stimulation session (Fig. 2). Only the second imaging session (i.e., stimulation session) received holographic stimulation on the pre-selected 5 target cells for 30 revolutions of 15 um spiral for about 100 ms at 5 mW laser power per cell (16 kHz target cell or 54 kHz target cell stimulation conditions) or 0 mW laser power per cell (control condition). To minimize any effect of external mechanic sounds to cells in the AC, we kept PMT shutter open during the imaging session. Number of imaging sessions per animal varied depending on the virus expression. Regardless, all animals were used for control and at least one stimulation condition with minimum 2 days apart by varying FOVs to avoid imaging the same cells multiple times. The order of conditions and the imaging depth presented to the same animal were randomized.

An additional single-cell stimulation only session was conducted on a subset of animals, to further test a reliable holographic stimulation at a single-cell level (n = 3 animals). We varied a stimulation position from the original target stimulation point to 10, 20, or 30 μm shifted along x-axis or y-axis, generating 7 different stimulation point (original cell position, 10, 20, or 30 μm shifted along the x-axis, 10, 20, or 30 μm shifted along the y-axis). We stimulated each stimulation point for 10 times in a randomized order across stimulation points with 8-sec. ISIs.

Analysis

Imaging data were processed with 'suite2p' for motion correction, cell detection, and cell fluorescence trace extraction [54]. We applied neuropil correction to the fluorescence traces using the following equation: $F_{(cell_corrected)} = F_{(cell)} - (0.8 * F_{(neuropil)})$. We then computed ΔF/F normalized to the baseline, by following the equation: $\Delta F/F = (F_{(trace)} - F_{(baseline)}) / F_{(baseline)}$, where baseline is about 300 ms before the sound onset. For the single-cell level stimulation session, we computed peak ΔF/F per each stimulation point and applied a mixed-effect model by taking peak ΔF/F as dependent variables, stimulation point as independent variables, and cells as random factor. For the 5-cell stimulation validation session, we computed a proportion of activated cells (any cell with peak $\Delta F/F > 0$) among stimulated cells per each FOV as well as peak ΔF/F and ran a random permutation with 100 iterations.

For experimental sessions, to select sound responsive cells, we compared sound-evoked activity (160 ms – 660 ms after sound onset) and the baseline activity (300 ms – 0 ms before the sound onset). We considered cells sound responsive when the amplitude of the average sound-evoked activity exceeded two standard deviations of the amplitude of the average baseline activity. Sound responsive cells were selected based on fluorescence traces only from the baseline session to minimize any potential effect of stimulation on cell selection. We then computed the ratio of the evoked activity between two frequencies as an index of the frequency preference ($\Delta F/F_{(16kHz)} - \Delta F/F_{(54kHz)}$). We subgrouped sound-responsive cells into either 16 kHz preferring cells or 54 kHz preferring cells based on the frequency preference, taking 0 as a subgroup criterion. As our main interest was changes to non-target cells, we excluded target cells for further analyses. To compare response changes due to stimulation for each group of cells, average sound-evoked activity of sound-responsive cells from the baseline session was subtracted from the stimulation session (stimulation effect: $\Delta F/F_{(stimulation\ session)} - \Delta F/F_{(baseline\ session)}$) for each condition. We further compared response changes between post-stimulation session and stimulation session, again by subtracting the response amplitudes between two sessions for each group and condition (post-stimulation effect: $\Delta F/F_{(post-stimulation\ session)} - \Delta F/F_{(stimulation\ session)}$). To quantify the stimulation effect based on functional properties for conditions and groups, we applied a mixed-effect model by taking amplitude changes as dependent variables, frequency and conditions as independent variables, and FOVs as random factor, for each group. We then computed repeated-measures analysis of variance (RM ANOVA) to examine whether the effect of functional property (frequency) to the amplitude changes was specific to the target frequency presentation synchronized with the stimulation (i.e., 16 kHz for 16 kHz target cell stimulation or 54 kHz for 54 kHz target cell stimulation). To quantify whether the response amplitude changes due to stimulation differ across trials, we fitted a dataset of average stimulation effect across each trial per each condition (stimulation or control), each cell group (16 kHz preferring or 54 kHz preferring cells), and each tone presentation (16 kHz or 54 kHz) to the three-parameter model and computed the extra sum-of-squares *F*-test to compare whether response amplitude changes across trials were different from a constant line [55]. To quantify a relationship between response amplitude changes of non-target cells and their distances to target cells, we computed a minimum distance of each cell position relative to any of target cells, and fitted the dataset of the response amplitude changes across distance to the three-parameter model to compute the extra sum-of-squares *F*-test, per each condition (16 kHz target stimulation, 54 kHz target stimulation, or control), each cell group (16 kHz preferring or 54 kHz preferring cells), and each tone presentation (16 kHz or 54 kHz). For the control condition, as there was no stimulated target cells, we chose top five most tone-responsive cells from the baseline session as "target" cells.

Histology

Animals were deeply anesthetized with 4% isoflurane to perform transcardial perfusion with 4% paraformaldehyde (PFA) in 0.1 M phosphate buffer saline (PBS). The extracted brains were post-fixed in 4% PFA for additional 12-24 hours. Coronal brain sections at 50 μm containing the AC were stained with primary antibodies of HA-Tag (1:500) and chicken Green Fluorescent Protein (GFP, 1:500) for GCaMP8s, and secondary antibodies of 594-conjugated anti-rabbit IgG (1:1000) and 488-conjugated anti-chicken IgG (1:1000) for red-shifted opsins.

References

1. Read, H., Winer, J., and Schreiner, C. (2001). Modular organization of intrinsic connections associated with spectral tuning in cat auditory cortex. Proceedings of the National Academy of Sciences of the United States of America *98*, 8042-8047. 10.1073/pnas.131591898.
2. Schnupp, J., Mrsic-Flogel, T., and King, A. (2001). Linear processing of spatial cues in primary auditory cortex. Nature *414*, 200-204. 10.1038/35102568.
3. Lu, K., Liu, W., Zan, P., David, S.V., Fritz, J.B., and Shamma, S.A. (2018). Implicit Memory for Complex Sounds in Higher Auditory Cortex of the Ferret. J Neurosci *38*, 9955-9966. 10.1523/JNEUROSCI.2118-18.2018.
4. Fritz, J., Shamma, S., Elhilali, M., and Klein, D. (2003). Rapid task-related plasticity of spectrotemporal receptive fields in primary auditory cortex. Nature Neuroscience *6*, 1216-1223. 10.1038/nn1141.
5. Bandyopadhyay, S., Shamma, S.A., and Kanold, P.O. (2010). Dichotomy of functional organization in the mouse auditory cortex. Nat Neurosci *13*, 361-368. 10.1038/nn.2490.
6. Rothschild, G., Nelken, I., and Mizrahi, A. (2010). Functional organization and population dynamics in the mouse primary auditory cortex. Nature Neuroscience *13*, 353-U321. 10.1038/nn.2484.
7. Panzeri, S., Macke, J., Gross, J., and Kayser, C. (2015). Neural population coding: combining insights from microscopic and mass signals. Trends in Cognitive Sciences *19*, 162-172. 10.1016/j.tics.2015.01.002.
8. Bowen, Z., Winkowski, D., and Kanold, P. (2020). Functional organization of mouse primary auditory cortex in adult C57BL/6 and F1 (CBAxC57) mice. Scientific Reports *10*, ARTN 10905. 10.1038/s41598-020-67819-4.
9. Francis, N., Winkowski, D., Sheikhattar, A., Armengol, K., Babadi, B., and Kanold, P. (2018). Small Networks Encode Decision-Making in Primary Auditory Cortex. Neuron *97*, 885-+. 10.1016/j.neuron.2018.01.019.
10. Francis, N., Mukherjee, S., Kocillari, L., Panzeri, S., Babadi, B., and Kanold, P. (2022). Sequential transmission of task-relevant information in cortical neuronal networks. Cell Reports *39*, ARTN 110878. 10.1016/j.celrep.2022.110878.
11. Hromádka, T., Deweese, M.R., and Zador, A.M. (2008). Sparse representation of sounds in the unanesthetized auditory cortex. PLoS Biol *6*, e16. 10.1371/journal.pbio.0060016.
12. Hromadka, T., and Zador, A. (2009). Representations in auditory cortex. Current Opinion in Neurobiology *19*, 430-433. 10.1016/j.conb.2009.07.009.
13. Liang, F., Li, H., Chou, X., Zhou, M., Zhang, N., Xiao, Z., Zhang, K., Tao, H., and Zhang, L. (2019). Sparse Representation in Awake Auditory Cortex: Cell-type Dependence, Synaptic Mechanisms, Developmental Emergence, and Modulation. Cerebral Cortex *29*, 3796-3812. 10.1093/cercor/bhy260.
14. Yu, L., and Yu, Y. (2017). Energy-Efficient Neural Information Processing in Individual Neurons and Neuronal Networks. Journal of Neuroscience Research *95*, 2253-2266. 10.1002/jnr.24131.
15. Jadi, M., and Sejnowski, T. (2014). Cortical oscillations arise from contextual interactions that regulate sparse coding. Proceedings of the National Academy of Sciences of the United States of America *111*, 6780-6785. 10.1073/pnas.1405300111.
16. Grabner, R., Neubauer, A., and Stern, E. (2006). Superior performance and neural efficiency: The impact of intelligence and expertise. Brain Research Bulletin *69*, 422-439. 10.1016/j.brainresbull.2006.02.009.

17. Bowen, Z., Winkowski, D.E., Seshadri, S., Plenz, D., and Kanold, P.O. (2019). Neuronal Avalanches in Input and Associative Layers of Auditory Cortex. Front Syst Neurosci *13*, 45. 10.3389/fnsys.2019.00045.
18. Chettih, S.N., and Harvey, C.D. (2019). Single-neuron perturbations reveal feature-specific competition in V1. Nature *567*, 334-340. 10.1038/s41586-019-0997-6.
19. LaFosse, P.K., Zhou, Z., O'Rawe, J.F., Friedman, N.G., Scott, V.M., Deng, Y., and Histed, M.H. (2024). Single-cell optogenetics reveals attenuation-by-suppression in visual cortical neurons. bioRxiv. 10.1101/2023.09.13.557650.
20. Adesnik, H., and Abdeladim, L. (2021). Probing neural codes with two-photon holographic optogenetics. Nat Neurosci *24*, 1356-1366. 10.1038/s41593-021-00902-9.
21. Yang, W., and Yuste, R. (2021). Holographic Imaging and Stimulation of Neural Circuits. Optogenetics: Light-Sensing Proteins and Their Applications in Neuroscience and Beyond, 613-639.
22. LaFosse, P., Zhou, Z., Friedman, N., Deng, Y., Li, A., Akitake, B., and Histed, M. (2023). Bicistronic Expression of a High-Performance Calcium Indicator and Opsin for All-Optical Stimulation and Imaging at Cellular Resolution. Eneuro *10*. 10.1523/ENEURO.0378-22.2023.
23. Sridharan, S., Gajowa, M., Ogando, M., Jagadisan, U., Abdeladim, L., Sadahiro, M., Bounds, H., Hendricks, W., Turney, T., Tayler, I., et al. (2022). High-performance microbial opsins for spatially and temporally precise perturbations of large neuronal networks. Neuron *110*, 1139-+. 10.1016/j.neuron.2022.01.008.
24. Mardinly, A., Oldenburg, I., Pegard, N., Sridharan, S., Lyall, E., Chesnov, K., Brohawn, S., Waller, L., and Adesnik, H. (2018). Precise multimodal optical control of neural ensemble activity. Nature Neuroscience *21*, 881-+. 10.1038/s41593-018-0139-8.
25. Daie, K., Svoboda, K., and Druckmann, S. (2021). Targeted photostimulation uncovers circuit motifs supporting short-term memory. Nature Neuroscience *24*, 259-265. 10.1038/s41593-020-00776-3.
26. Kane, K.L., Longo-Guess, C.M., Gagnon, L.H., Ding, D., Salvi, R.J., and Johnson, K.R. (2012). Genetic background effects on age-related hearing loss associated with Cdh23 variants in mice. Hear Res *283*, 80-88. 10.1016/j.heares.2011.11.007.
27. Branchi, I., Santucci, D., and Alleva, E. (2001). Ultrasonic vocalisation emitted by infant rodents: a tool for assessment of neurobehavioural development. Behav Brain Res *125*, 49-56. 10.1016/s0166-4328(01)00277-7.
28. Froemke, R., and Hyman, S. (2015). Plasticity of Cortical Excitatory-Inhibitory Balance. Annual Review of Neuroscience, Vol 38 *38*, 195-219. 10.1146/annurev-neuro-071714-034002.
29. Karmarkar, U., and Buonomano, D. (2007). Timing in the absence of clocks: Encoding time in neural network states. Neuron *53*, 427-438. 10.1016/j.neuron.2007.01.006.
30. Liu, B., Seay, M., and Buonomano, D. (2023). Creation of Neuronal Ensembles and Cell-Specific Homeostatic Plasticity through Chronic Sparse Optogenetic Stimulation. Journal of Neuroscience *43*, 82-92. 10.1523/JNEUROSCI.1104-22.2022.
31. Hebb, D.O. (2005). The organization of behavior: A neuropsychological theory (Psychology press).
32. Malenka, R.C., and Nicoll, R.A. (1999). Long-term potentiation--a decade of progress? Science *285*, 1870-1874. 10.1126/science.285.5435.1870.
33. Brown, T.H., Kairiss, E.W., and Keenan, C.L. (1990). Hebbian synapses: biophysical mechanisms and algorithms. Annual review of neuroscience *13*, 475-511.

34. Vitureira, N., and Goda, Y. (2013). The interplay between Hebbian and homeostatic synaptic plasticity. Journal of Cell Biology *203*, 175-186. 10.1083/jcb.201306030.
35. Fox, K., and Stryker, M. (2017). Integrating Hebbian and homeostatic plasticity: introduction. Philosophical Transactions of the Royal Society B-Biological Sciences *372*, ARTN 20160413. 10.1098/rstb.2016.0413.
36. Toyoizumi, T., Kaneko, M., Stryker, M., and Miller, K. (2014). Modeling the Dynamic Interaction of Hebbian and Homeostatic Plasticity. Neuron *84*, 497-510. 10.1016/j.neuron.2014.09.036.
37. Turrigiano, G., and Nelson, S. (2000). Hebb and homeostasis in neuronal plasticity. Current Opinion in Neurobiology *10*, 358-364. 10.1016/S0959-4388(00)00091-X.
38. Yin, J., and Yuan, Q. (2015). Structural homeostasis in the nervous system: a balancing act for wiring plasticity and stability. Frontiers in Cellular Neuroscience *8*, ARTN 439. 10.3389/fncel.2014.00439.
39. Maor, I., Shalev, A., and Mizrahi, A. (2016). Distinct Spatiotemporal Response Properties of Excitatory Versus Inhibitory Neurons in the Mouse Auditory Cortex. Cerebral Cortex *26*, 4242-4252. 10.1093/cercor/bhw266.
40. Wang, Y., Ye, M., Kuang, X., Li, Y., and Hu, S. (2018). A simplified morphological classification scheme for pyramidal cells in six layers of primary somatosensory cortex of juvenile rats. Ibro Reports *5*, 74-90. 10.1016/j.ibror.2018.10.001.
41. Marin, O. (2012). Interneuron dysfunction in psychiatric disorders. Nature Reviews Neuroscience *13*, 107-120. 10.1038/nrn3155.
42. Xu, J., Fan, J., Wang, X., Eacker, S., Kam, T., Chen, L., Yin, X., Zhu, J., Chi, Z., Jiang, H., et al. (2016). Cultured networks of excitatory projection neurons and inhibitory interneurons for studying human cortical neurotoxicity. Science Translational Medicine *8*, ARTN 333ra48. 10.1126/scitranslmed.aad0623.
43. Wonders, C., and Anderson, S. (2006). The origin and specification of cortical interneurons. Nature Reviews Neuroscience *7*, 687-696. 10.1038/nrn1954.
44. Nathanson, J., Yanagawa, Y., Obata, K., and Callaway, E. (2009). Preferential Labeling of Inhibitory and Excitatory Cortical Neurons by Endogenous Tropism of Adeno-associated Virus and Lentivirus Vectors. Neuroscience *161*, 441-450. 10.1016/j.neuroscience.2009.03.032.
45. Wehr, M., and Zador, A.M. (2003). Balanced inhibition underlies tuning and sharpens spike timing in auditory cortex. Nature *426*, 442-446.
46. Bittner, S., Williamson, R., Snyder, A., Litwin-Kumar, A., Doiron, B., Chase, S., Smith, M., and Yu, B. (2017). Population activity structure of excitatory and inhibitory neurons. Plos One *12*, ARTN e0181773. 10.1371/journal.pone.0181773.
47. Chen, I.W., Helmchen, F., and Lütcke, H. (2015). Specific early and late oddball-evoked responses in excitatory and inhibitory neurons of mouse auditory cortex. Journal of Neuroscience *35*, 12560-12573.
48. Li, J.Y., and Glickfeld, L.L. (2023). Input-specific synaptic depression shapes temporal integration in mouse visual cortex. Neuron. 10.1016/j.neuron.2023.07.003.
49. Davis, G. (2013). Homeostatic Signaling and the Stabilization of Neural Function. Neuron *80*, 718-728. 10.1016/j.neuron.2013.09.044.
50. Tien, N., Soto, F., and Kerschensteiner, D. (2017). Homeostatic Plasticity Shapes Cell-Type-Specific Wiring in the Retina. Neuron *94*, 656-+. 10.1016/j.neuron.2017.04.016.
51. Maffei, A., and Fontanini, A. (2009). Network homeostasis: a matter of coordination. Current Opinion in Neurobiology *19*, 168-173. 10.1016/j.conb.2009.05.012.

52. Barak, O., and Tsodyks, M. (2007). Persistent activity in neural networks with dynamic synapses. Plos Computational Biology *3*, 323-332, ARTN e35. 10.1371/journal.pcbi.0030035.
53. Liu, J., Whiteway, M.R., Sheikhattar, A., Butts, D.A., Babadi, B., and Kanold, P.O. (2019). Parallel Processing of Sound Dynamics across Mouse Auditory Cortex via Spatially Patterned Thalamic Inputs and Distinct Areal Intracortical Circuits. Cell Rep *27*, 872-885.e877. 10.1016/j.celrep.2019.03.069.
54. Pachitariu, M., Stringer, C., Schröder, S., Dipoppa, M., Rossi, L.F., Carandini, M., and Harris, K.D. (2016). Suite2p: beyond 10,000 neurons with standard two-photon microscopy. BioRxiv, 061507.
55. Motulsky, H., and Christopoulos, A. (2004). Fitting models to biological data using linear and nonlinear regression: a practical guide to curve fitting (Oxford University Press).

Acknowledgments: Supported by U19 NS107464 (POK), NIH RO1DC017785 (POK), NIH F32DC019842 (TAB).

Author Contributions: Conceptualization: HK, TAB, POK; Methodology: HK, TAB, POK; Investigation: HK, TAB; Writing: HK, POK

Competing interest: Authors declare that they have no competing interests.

Data and materials availability: All preprocessed imaging data and relevant analyses scripts will be deposited at Johns Hopkins University research data repository, available for open access.

Figures

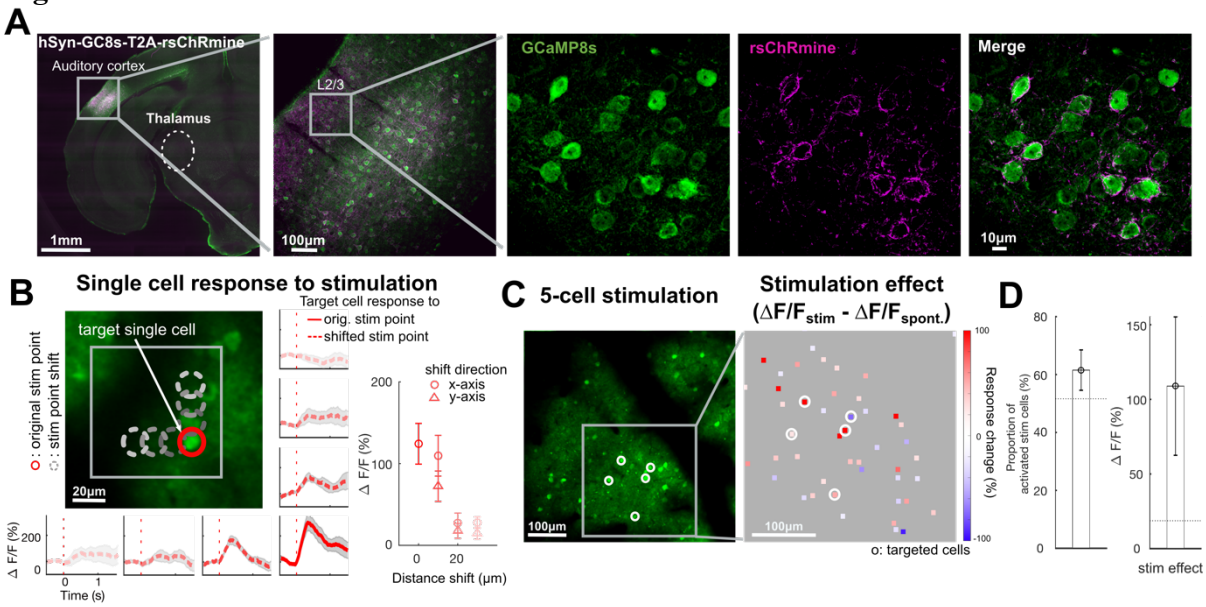

Figure 1. Holographic optogenetic stimulation manipulates cell activity in AC. A: An example brain slice showing cells in AC expressing both GCaMP and opsin (AAV9-hSyn-GC8s-T2A-rsChRmine). **B**: An example field of view (FOV) where single cell targeting precision was tested and response traces to the holographic stimulation from an example cell. Stimulation was offset from the original position (red circle) to distance-shifted positions in 10 μm increments (gray dashed circles in the x-axis or y-axis of the FOV). Responses were the greatest when the stimulation was performed on the original cell position (red solid line trace). Rapid amplitude decay along the position shift was observed (red dashed line traces). Grey error shades indicate SEM across trials. A right inset errorbar plot shows a grand average amplitude change per stimulation point across all tested cells (n = 15 cells, 3 animals). Error bars indicate SEM across cells. **C**: An example FOV showing a population of cells (left) and amplitude changes to 5-cell stimulation as a stimulation effect ($\Delta F/F_{stim} - \Delta F/F_{spont., right}$). Filled squares indicate each cell. White circles indicate stimulation targeted cells. **D**: (left) Proportion of stimulated cells that showed an increase in fluorescence following photostimulation. Error bars indicate SEM across FOVs. A horizontal dashed line indicates average permutation results (random permutation test on 100 iterations, $p < 0.0001$). (right) Grand average of the stimulation effect across imaging sessions. Error bars indicate SEM across FOVs. A horizontal dashed line indicates average permutation results (random permutation test on 100 iterations, $p < 0.0001$).

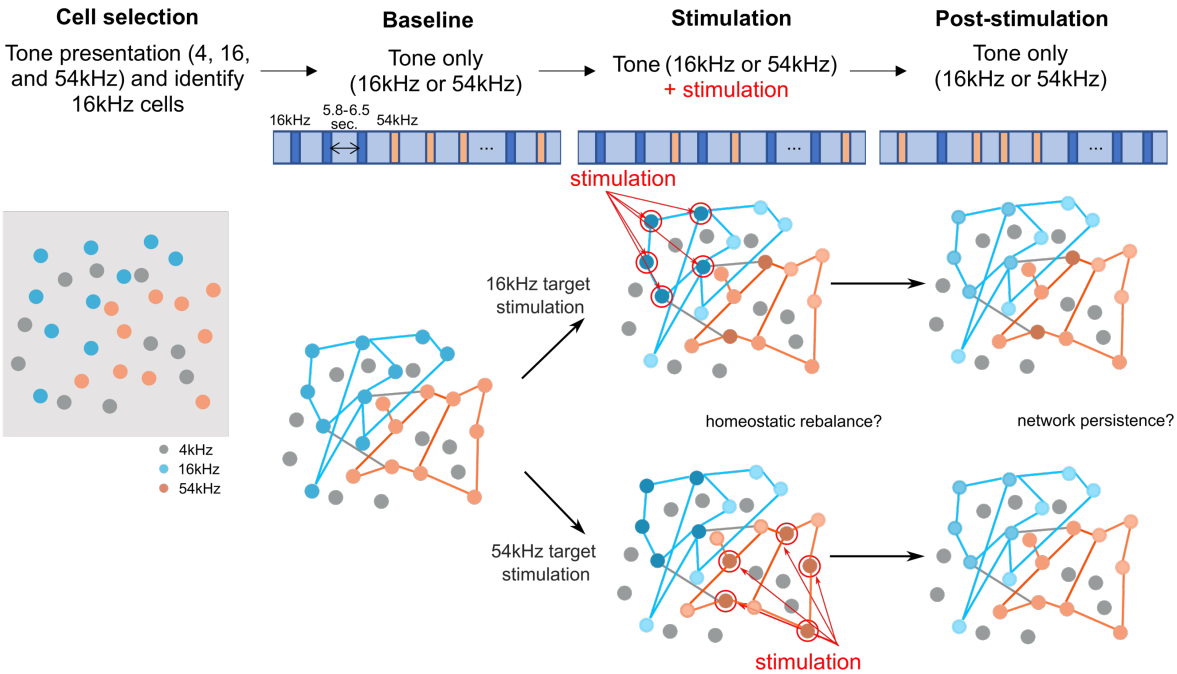

Figure 2. Experimental procedure. A total of four consecutive imaging sessions were acquired: 1) A cell selection session to identify neurons selective for 16 kHz pure tones, 2) a baseline imaging session to acquire tone-evoked activity response to either 16 or 54 kHz pure tone, 3) a stimulation session representing five cells of either 16 kHz or 54 kHz responsive cells as target stimulation to examine the effect of stimulation synchronized to tone presentations, and 4) a post-stimulation session to examine network persistence after stimulation-related changes.

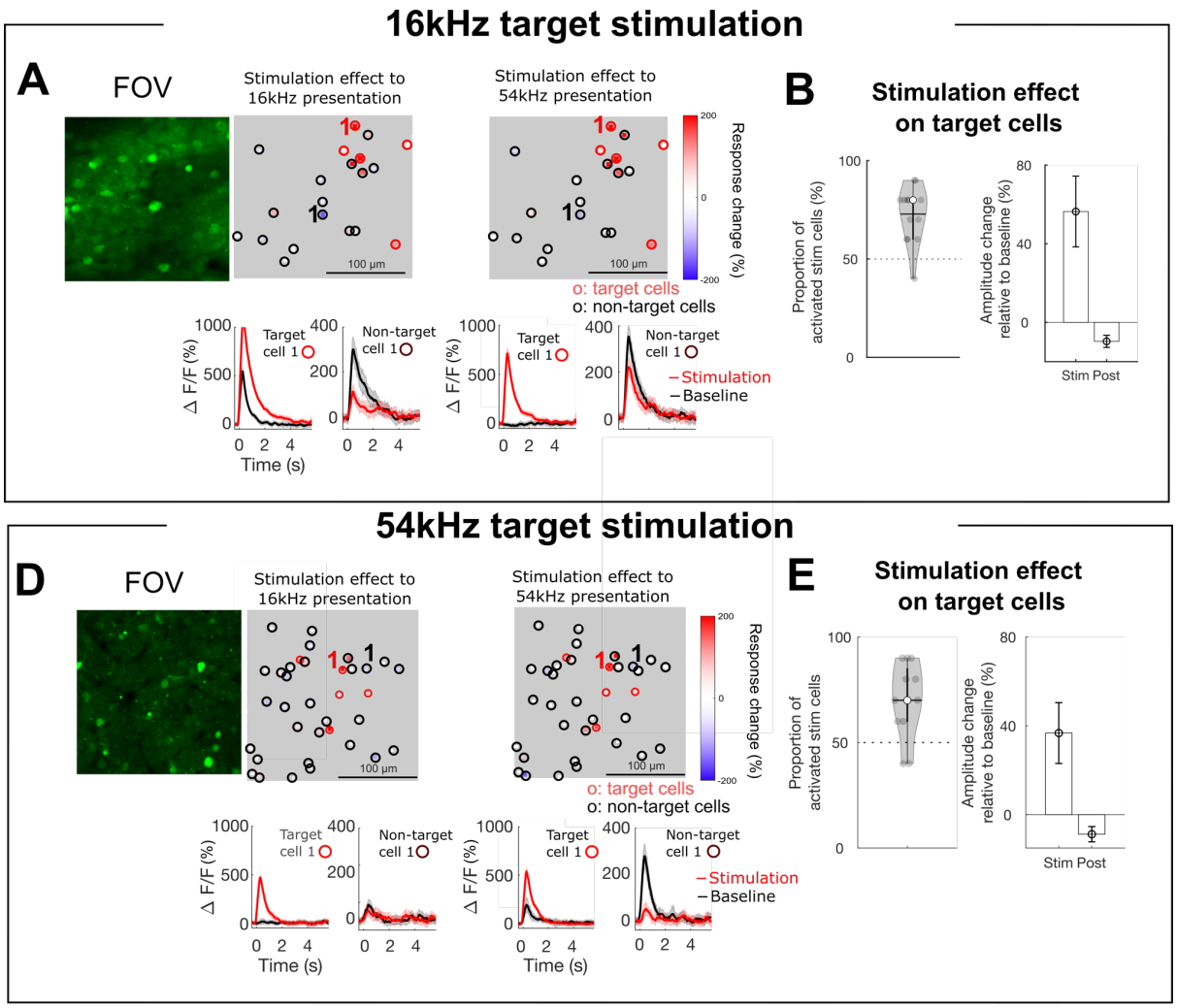

Figure 3. Targeted cells and non-targeted cells show response changes due to stimulation. **A**: (top) An example FOV showing the stimulation effect ($\Delta F/F_{stim} - \Delta F/F_{baseline}$) of sound responsive cells for 16 kHz target cell stimulation (filled squares). Black circles indicate stimulated target cells. (bottom) Mean response traces of an example target and non-target cell in baseline session (black) and stimulation session (red). Error bars indicate SEM across trials. An example target cell shows an increased response due to the stimulation. An example non-target cell shows a decreased response due to stimulation on the target cells. **B**: (left) A violin plot of the proportion of stimulated cells that showed increased activity due to stimulation across FOVs. Horizontal solid line indicates mean proportion, empty circle indicates median proportion, and gray filled circles indicate individual FOVs. (right) Mean amplitude changes of target cells for stimulation session and post-stimulation session normalized to the baseline session. Error bars indicate SEM across cells. Dashed horizontal lines on both panels indicate average permutation results (random permutation test on 100 iterations, $p < 0.0001$). **DE**: Same as ABC for 54 kHz target cell stimulation.

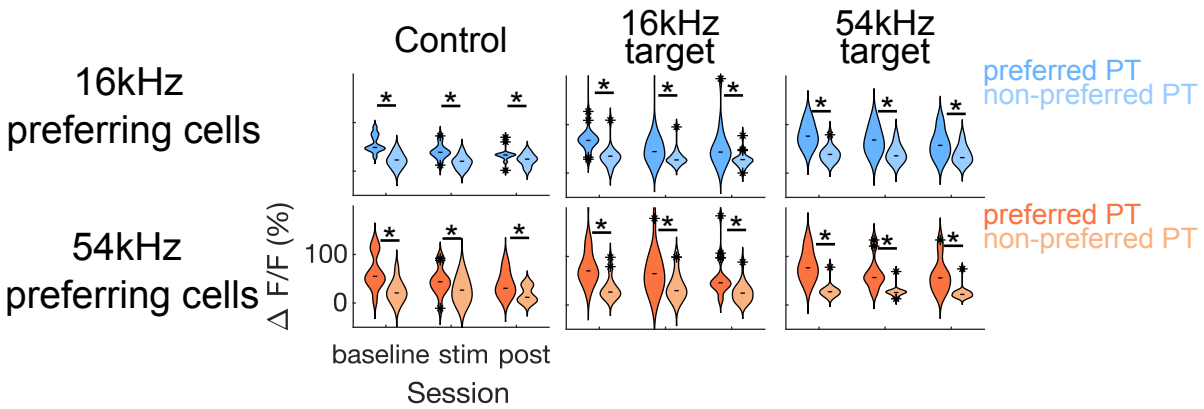

Figure 4. Subgrouped non-target cells show the frequency preference. Violin plots for average response amplitudes of either 16 kHz preferring cells (blue) or 54 kHz preferring cells (orange) to each frequency for each session and for each condition (either 16kHz 5-cell stimulation, 54kHz 5-cell stimulation, or control with no stimulation at each column). Both groups of cells show greater responses to their preferred frequency (darker shades) regardless of the session (Asterisks above the horizontal line; Mixed-effect model, $p < 0.0001$ for frequency, all $p > 0.05$ across sessions and conditions). Asterisks on the violinplot indicate outlier cells and horizontal lines on the the violinplot indicate medians.

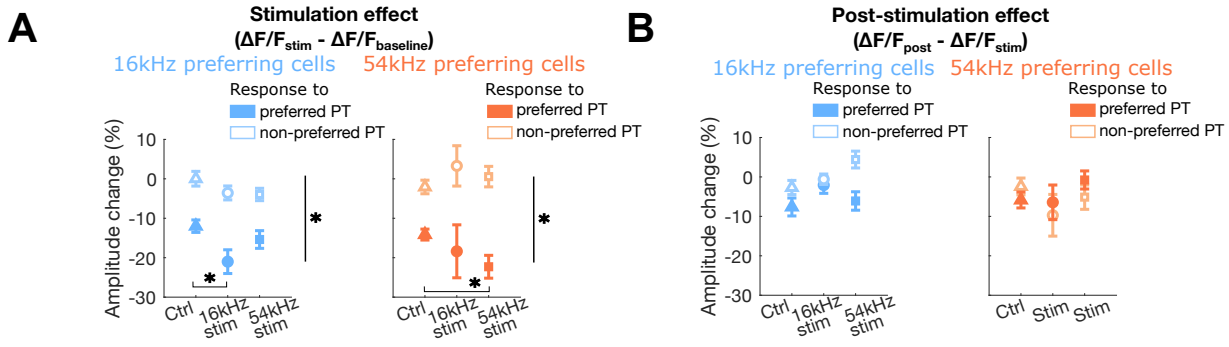

Figure 5. Non-target co-tuned cells show more decreased response amplitudes due to stimulation when synchronized with their preferred tones. A: Stimulation effect ($\Delta F/F_{stim} - \Delta F/F_{baseline}$) in 16 kHz (blue) and 54 kHz (orange) preferring cells. Both cell groups show decreased amplitude to their preferred frequency regardless of conditions due to acoustic stimulus-specific adaptation. Only co-tuned cells (16 kHz preferring cells for 16 kHz stimulation or 54 kHz preferring cells for 54 kHz stimulation) show a further decrease in response amplitudes due to the stimulation, when the preferred pure tone (PT) frequency was synchronized. Error bars indicate SEM across FOVs (*: $p = 0.01$, **: $p < 0.0001$). **B**: Post-stimulation effect ($\Delta F/F_{post} - \Delta F/F_{stim}$) 16 kHz (blue) and 54 kHz (orange) preferring cells. No significant response amplitude changes were observed. Error bars indicate SEM across FOVs.

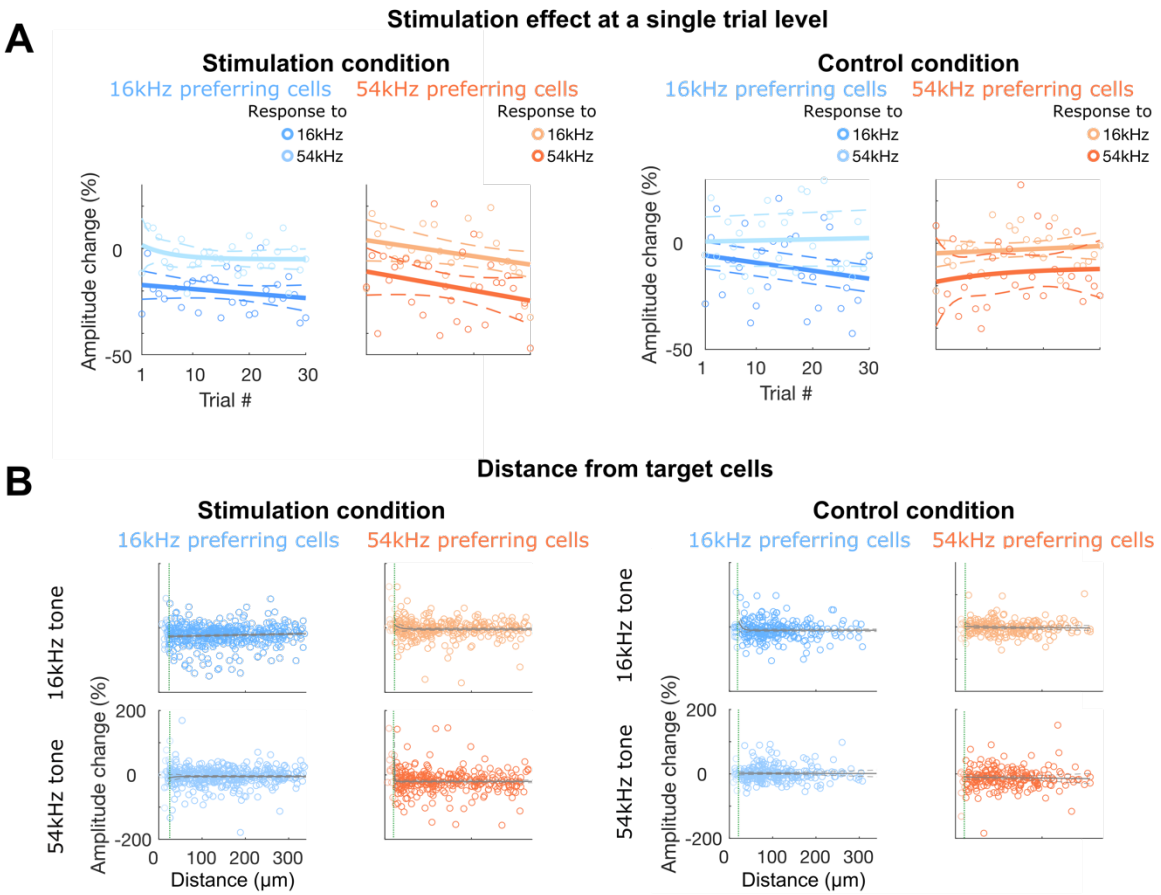

Figure 6. Rebalanced response changes on non-target 16 kHz cells are immediate and widely distributed. A: Stimulation effect ($\Delta F/F_{stim} - \Delta F/F_{baseline}$) in 16 kHz (blue) and 54 kHz (orange) preferring cells per each trial for the 5-cell stimulation condition (left) and the no-cell control condition (right). Decreased amplitudes to preferred frequencies were observed from as early as trial 1 with no significant further changes across trials, regardless of frequencies and conditions (sum-of-squares *F*-test, all $p > 0.05$). Solid lines indicate fitted curves and dashed lines indicate 95% confidence intervals. **B**: Stimulation effect ($\Delta F/F_{stim} - \Delta F/F_{baseline}$) of each non-target 16 kHz (blue) or 54 kHz (orange) preferring cells for either 16 kHz (top row) or 54 kHz (bottom row) presentation in relation to the minimum distance to any target cells for the stimulation condition (left) and the control condition (right). For the control condition, we considered top 5 most tone-responsive cells from the baseline session as "*target*" cells, as there was no stimulation. Non-target cells are widely distributed within the FOV (550 μm^2), regardless of cell groups, frequencies, and conditions. Gray lines indicate fitted curves, excluding cells that are closer than 15 μm (vertical green lines; cells < 15 μm marked in lighter shades), and dashed lines indicate 95% confidence intervals.

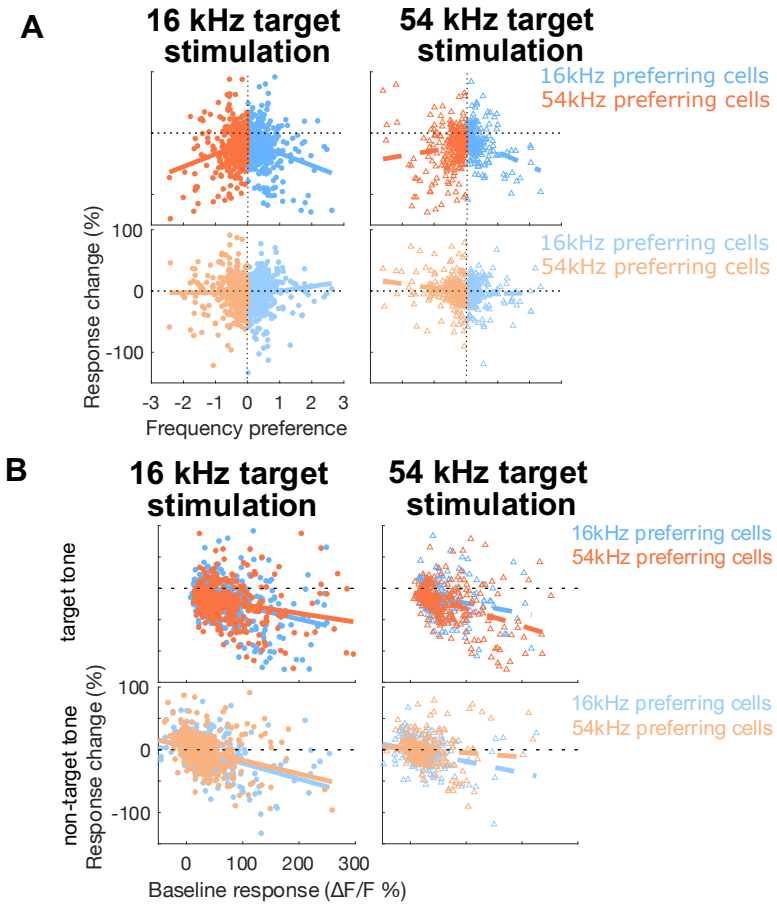

Figure 7. Stimulation effect is not dependent on the frequency tuning or baseline response amplitudes. A: Response change between the stimulation and baseline session (i.e., stimulation effect) relative to the frequency preference (negative values for 54 kHz preference, positive values for 16 kHz preference). While cells that showed greater response changes showed greater preference to their preferred frequency presentation, no difference between target ensemble conditions was observed. **B:** Response changes relative to the baseline response amplitudes. Similar to the frequency preference, no significant difference between cell groups and target ensemble conditions were observed.